

Quantum Reactive Scattering in Three Dimensions using
Hyperspherical (APH) Coordinates: Periodic Distributed
Approximating Functional (PDAF) Method for Surface Functions

Keming Zhang, Gregory A. Parker*

Department of Physics and Astronomy

University of Oklahoma, Norman, OK 73019

Donald J. Kouri†

Department of Chemistry and Department of Physics

University of Houston, Houston, TX 77204-5641

David K. Hoffman‡

Department of Chemistry and Ames Laboratory,

Iowa State University, Ames, IA 50011

and

Srinivasan S. Iyengar

The Henry Eyring Center for Theoretical Chemistry and Department of Chemistry

The University of Utah, Salt Lake City, UT 84112

July 22, 2002

Periodic distributed approximating functionals (PDAFs) are proposed and used to obtain a coordinate representation for the Adiabatically Aadjusting Pincipal Axis Hyperspherical (APH) coordinate kinetic energy operator. The approach is tested and accurate results for adiabatic surface functions for the reaction $F+H_2 \rightarrow HF+H$ are calculated and compared to those of some existing methods.

*Supported under National Science Foundation Grant CHE-9710383 and PHY-0100704.

†Supported under National Science Foundation Grant CHE-0074311 and R. A. Welsch Foundation Grant E-0608.

‡The Ames Laboratory is supported by the Department of Energy under Contract No 2-7405-ENG82

1 Introduction

As is well known [1, 2, 3, 4, 5, 6, 7, 8, 9, 10, 11], there has been tremendous progress in recent years in accurate quantum calculations on exchange (rearrangement) reactions of the form



and these now include cases in which four atoms [12] are present (*i.e.*, where C is replaced by CD in the above reactions) as well as the above three atom reaction. Many of these methods use hyperspherical coordinates and are efficient; however, the accurate solution of the quantum Schrödinger equation continues to be computationally intensive. Hence, there is a real need to make the codes more efficient and accurate, especially if one is interested in collisions involving multiple electronic states or collision-induced dissociation.

In the hyperspherical coordinate formulation of triatomic reactive scattering, composed of a hyperradius and five angular coordinates, the total wave function is expanded in a complete set of products of Wigner D-functions for the three Euler angles “external angles” describing the spatial orientation of the three-particle plane, times basis functions or surface functions which depend on the remaining two “internal” hyperspherical angles. The dependence of the expansion coefficients on the hyperradius, which is a measure of the size of the three particle system, is then determined by propagating the solution of a set of coupled-channel(CC) differential equations from a small hyperradius, where the solutions must be regular because the atoms coalesce, to a large hyperradius where the wavefunction is projected onto the arrangement channels and analytic boundary conditions are used to determine the scattering matrix. In the methods using hyperspherical coordinates that treat all particles symmetrically[8, 13, 9, 10, 14, 15, 16, 17], one numerically obtains “surface functions,” the basis functions of the two hyperangles, by numerically solving a two-dimensional (2D) Schrödinger equation. This Schrödinger equation, which is discussed in more detail later in this paper (See Sec. 3), depends parametrically on the hyperradius and must be solved at many values of the hyperradius. In addition, a large number of surface functions must be obtained at each hyperradius, and hence efficient computational procedures for numerically solving this 2D Schrödinger equation are essential.

The first accurate fully three-dimensional (3D) reactive scattering calculations employing hyperspherical coordinates used finite element methods (FEMs)[9, 10, 14, 11, 17, 18, 19] to solve for the surface functions. Although these FEMs give fairly accurate results, they are inefficient and not robust. Another commonly used method involves the use of the discrete variable representation (DVR)[14, 15, 20, 21, 22], which is most efficient at small hyperradii where the surface functions are delocalized. At larger values of the hyperradius,

where the surface functions are highly localized, the DVR points cover the whole space, making the method much less efficient. In a few cases the DVR is even more expensive than the FEM because of the need for many grid points in a small, localized region. Other methods such as the finite basis representation (FBR)[8, 13, 16] of Launay and LeDourneuf, and the method of Wolniewicz and Hinze[23] are also efficient only at large hyperradii. The analytic basis method (ABM) uses primitive ro-vibrational basis functions centered in the arrangement channels, and provides a very compact representation and thus is quite efficient at large hyperradii, but is inefficient and the basis is overcomplete at small hyperradii.[24]

In this paper, we present the Periodic Distributed Approximating Functional (PDAF) method, an approach that is efficient at both small and large values of the hyperradius. The PDAF method is similar to the Symmetry-Adapted-Hermite Distributed Approximating Functional (SA-HDAF) approach of Iyengar, Parker, Kouri and Hoffman [25], but differs importantly by involving only real symmetric matrices. In addition, in the present approach only the surface functions are obtained, while in the SA-HDAF approach [25] the full 3D wavefunction was obtained directly, by using an iterative procedure. The symmetry adaptation of the PDAF is carried out here in a similar, but simpler, fashion than in Ref. [25]. Here we employ the Distributed Approximating Functional (DAF) concept, but the PDAF differs from all previous DAF's. However, like other DAF's it is both accurate and efficient as a computational tool. A more detailed exposition of the connections between the PDAF and the Christoffel-Darboux formula for DAFs based on orthogonal polynomials will follow [26]. The sequential diagonalization-truncation technique[27] is employed to project the large-size Hamiltonian matrix into a smaller matrix using a projection matrix which is obtained by solving a one-dimensional eigensystem, thus significantly reducing the memory requirements and the computation time.

This paper is organized as follows. In Sec. 2 we introduce the PDAFs and derive their formulae. In Sec. 3 the ro-vibrational triatomic Hamiltonian in the APH coordinates system is presented and the symmetrization and reductions of the Hamiltonian are illustrated. The PDAF approach is then tested in Sec. 4. Surface functions for the FH₂ scattering system are computed, and the eigen-energies and the matrix elements are calculated and compared to those of existing methods (FEM, ABM and DVR) in Sec. 5. In Sec. 6 we present our conclusions.

2 Periodic Distributed Approximating Function (PDAF)

From the definition of the Dirac Delta function we know that

$$f(x) = \int_{-\infty}^{\infty} \delta(x - x')f(x')dx' \quad (2)$$

for any continuous function $f(x)$. Consider periodic functions, $f_p(x)$, for convenience scaled to have period 2π . Expressing the integration range as an infinite sum of segments of length 2π we can write

$$f_p(x) = \sum_{m=-\infty}^{\infty} \int_0^{2\pi} \delta(x - x' - 2m\pi) f_p(x' + 2m\pi) dx'. \quad (3)$$

Interchanging the integral and sum, and using the periodicity of $f_p(x)$, we have

$$f_p(x) = \int_0^{2\pi} \sum_{m=-\infty}^{\infty} \delta(x - x' - 2m\pi) f_p(x') dx' \quad (4)$$

or

$$f_p(x) = \int_0^{2\pi} \delta_p(x - x') f_p(x') dx' \quad (5)$$

where

$$\delta_p(x - x') = \sum_{m=-\infty}^{\infty} \delta(x - x' - 2m\pi) \quad (6)$$

is the periodic delta function. Since $\delta(x)$ is an even function, it's easy to see that $\delta_p(x)$ is even and is also periodic with a period of 2π . The k^{th} derivative of $f_p(x)$ is then given by

$$f_p^{(k)}(x) = \int_0^{2\pi} \delta_p^{(k)}(x - x') f_p(x') dx'. \quad (7)$$

Expanding $\delta_p(x - x')$ in a Fourier series,

$$\delta_p(x - x') = \frac{a_0}{2} + \sum_{n=1}^{\infty} a_n \cos n(x - x') \quad (8)$$

and using the identities

$$\int_0^{2\pi} \cos m(x - x') \cos nx' dx' = \begin{cases} \delta_{mn} \pi \cos nx & n \neq 0 \\ \delta_{mn} 2\pi & n = 0 \end{cases} \quad (9)$$

$$\int_0^{2\pi} \cos m(x - x') \sin nx' dx' = \delta_{mn} \pi \sin nx \quad (10)$$

we obtain

$$a_n = \frac{1}{\pi}, \quad n = 0, 1, 2, \dots \quad (11)$$

Thus, we obtain

$$\delta_p(x - x') = \frac{1}{\pi} \left(\frac{1}{2} + \sum_{n=1}^{\infty} \cos n(x - x') \right), \quad (12)$$

for the periodic delta function.

We define the partial sum of the periodic delta function to be the continuous Periodic Distributed Approximating Function (PDAF)

$$\delta_{p,M}(x-x') \equiv \frac{1}{\pi} \left[\frac{1}{2} + \sum_{n=1}^M \cos n(x-x') \right] = \frac{1}{2\pi} \left\{ \frac{\cos[(M-1)(x-x')] - \cos[M(x-x')]}{1 - \cos(x-x')} \right\}, \quad (13)$$

which is the basic result used in this work. The last expression is obtained by noting that $\delta_{p,M}(x-x')$ is the real part of a sum of exponentials which can be written as a geometric sum and thus done analytically. By definition, as M increases the PDAF approaches the periodic delta function, *i.e.*

$$\delta_p(x-x') = \lim_{M \rightarrow \infty} \delta_{p,M}(x-x'). \quad (14)$$

One may obtain the fully discretized PDAF by approximating the integral over x' in Eq. (7) using a trapezoidal quadrature

$$f_{p,M}^{(k)}(x) = \sum_{j=1}^N \delta_{p,M}^{(k)}(x-x_j) f_p(x_j) \Delta x \quad (15)$$

where N is the number of grid points, $\Delta x = \frac{2\pi}{N}$ and $x_j = (j - \frac{1}{2})\Delta x$. This choice of quadrature points is particularly useful if we are solving differential equations with singular points at the two ends ($x = 0$ and $x = 2\pi$). As the grid points are fixed, $\delta_{p,M}^{(k)}(x)$ acts like the discretized k^{th} derivative operator. One can also discretize x using the same grid points as used in the numerical quadrature. If we treat the discretized $f_{p,M}(x)$ and it's derivatives as a column vectors *e. g.*, $[f_j = f(x_j)]$, we have

$$f_i^{(k)} = \sum_{j=1}^N D_{ij}^{(k)} f_j \quad (16)$$

where

$$D_{ij}^{(k)} = \delta_{p,M}^{(k)}(x_i - x_j) \Delta x = \begin{cases} (-1)^{\frac{k+1}{2}} \frac{\Delta x}{\pi} \sum_{n=1}^M n^k \sin n[(x_i - x_j)]x & k \text{ odd} \\ \frac{\Delta x}{2\pi} \delta_{0,k} + (-1)^{\frac{k}{2}} \frac{1}{\pi} \sum_{n=1}^M n^k \cos n[(x_i - x_j)] & k \text{ even} \end{cases} \quad (17)$$

is the k^{th} derivative operator in matrix form. The differential operators, $D^{(k)}$ are periodic Toeplitz matrices which depend on only one parameter M . As M increases, the PDAF gives an increasingly accurate representation of the Dirac delta function. However, it is for small M the integrand of Eq. (7) is smoothest and the trapezoidal rule is most accurate. Hence, we seek an optimal compromise value of M . Since, the

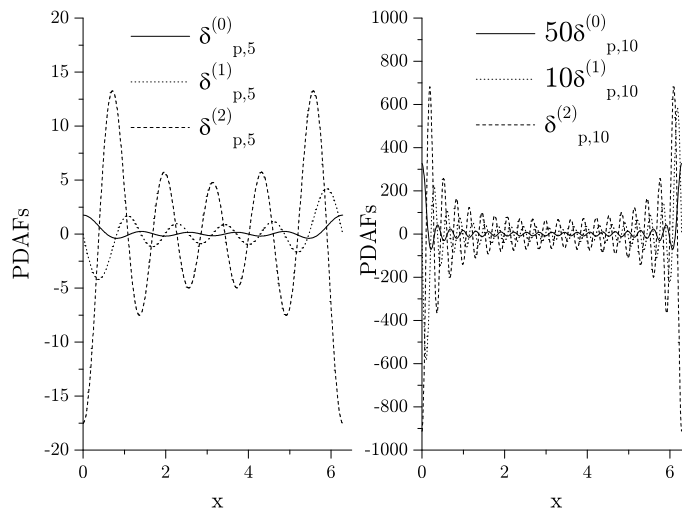


Figure 1: $\delta_{p,M}^{(k)}(x)$ for different M , where the number of grid points ($N = 20$) is used in both panels. In the left panel $M = 5$ and in the right panel $M = N/2 = 10$. Note $\delta_{p,M}^{(0)}$ and $\delta_{p,M}^{(2)}$ are symmetric about $x = 0$, while $\delta_{p,M}^{(1)}$ is anti-symmetric. Increasing M makes the PDAFs sharply peaked and a better representation of the respective delta function and its derivatives.

integrand involves a Fourier function, the theory of Gaussian quadrature suggests a relation of $M = N/2$. Through numerical experimentation (see Sec. 4) we verify that this value gives the most accurate results. In this paper, we will use $D^{(0)}$, $D^{(1)}$ and $D^{(2)}$, consequently we need $\delta_{p,M}^{(0)}$, $\delta_{p,M}^{(1)}$ and $\delta_{p,M}^{(2)}$. They can be obtained simply by differentiating Eq. (13).

We see that $\delta_{p,M}^{(k)}(x)$ are even(odd) periodic functions when k is even(odd). The functions, $\delta_{p,M}^{(0)}(x)$, $\delta_{p,M}^{(1)}(x)$, and $\delta_{p,M}^{(2)}(x)$ which are the ones used in this paper, are shown in Fig. 1. In both panels of Fig. 1 $N = 20$, in the left panel $M = 5$ and in the right panel $M = N/2 = 10$. One can readily see the symmetry of each PDAF. Comparing the left and right panels in Fig. 1 we see that increasing M makes the PDAFs in the right panel sharply peaked and a better approximate representation of the periodic Dirac Delta function and its derivatives.

The equations obtained in this section for the PDAF, namely Eq. (13) and Eq. (17), may be compared with those obtained using the SA-HDAF [25] for functions with periodic symmetry, namely Eq. (5) and associated expressions in Ref. [25]. It is clear that both representations are Toeplitz, however, the expression in Ref. [25] has the additional characteristic of being banded, which is not the case in the present formulation. However, as we will see later in this paper, this does not present any problems in the current implementation and in fact helps in enhance the accuracy of the procedure introduced here.

3 Symmetrization and Reductions of the Triatomic Hamiltonian in APH Coordinates

3.1 APH Hamiltonian

The detailed reactive scattering theory formulated in adiabatically adjusting principle axes hyperspherical (APH) coordinates has been presented previously[9], and we repeat only the essentials here. In this approach, one needs sector adiabatic basis functions $\Phi_{\tau\Lambda}^p$ of the APH hyperangles, and in this work we choose surface functions, $\Phi_{\tau\Lambda}^p$ defined by the equation

$$H\Phi_{\tau\Lambda}^p(\theta, \chi; \rho_\xi) = \mathcal{E}_{\tau\Lambda}^p(\rho_\xi)\Phi_{\tau\Lambda}^p(\theta, \chi; \rho_\xi) \quad (18)$$

where H is a portion of the full Hamiltonian omitting parts of the orbital angular momentum. Thus we take

$$H = -\frac{\hbar^2}{2\mu\rho_\xi^2} \left[\frac{4}{\sin 2\theta} \frac{\partial}{\partial\theta} \sin 2\theta \frac{\partial}{\partial\theta} + \frac{1}{\sin^2\theta} \frac{\partial^2}{\partial\chi^2} \right] + \frac{15\hbar^2}{8\mu\rho_\xi^2} + C\hbar^2\Lambda^2 + V(\rho_\xi, \theta, \chi). \quad (19)$$

The first term in the Hamiltonian H is the ‘‘hyperspherical’’ part of the kinetic energy operator, and

$$C = \frac{1}{\mu\rho_\xi^2(1 - \sin\theta)} \quad (20)$$

is part of the centrifugal potential. The potential energy V used here is the complete potential energy surface (PES) of Brown *et al.*[29], and the $\mathcal{E}_{\tau,\Lambda}^p(\rho_\xi)$ are the eigenenergies of H at the hyperradius ρ_ξ . The variable θ is the APH bending angle; its range is $0 \leq \theta \leq \pi/2$, with $\pi/2$ describing linear configurations and 0 describing triangular symmetric top configurations. The variable χ is the APH kinematic angle measured from the ‘‘incident’’ arrangement channel; it measures motion between arrangement channels, and its range is $-\pi \leq \chi \leq \pi$. The angles θ and χ cover the upper half of the surface of an internal coordinate sphere which we loosely call the ‘‘hypersphere’’. (More precisely, the surface of the hypersphere is the 5D space covered by θ , χ , and the three Euler angles which describe the orientation of the principal axes in space. In fact, the hypersphere may be decomposed into two commuting subgroups, $O(2)$ and $O(3)$, and this aspect has been exploited in computing surface functions with fixed total angular momentum. [9]) As one can see from Eq. (18), the surface functions $\Phi_{\tau,\Lambda}^p$ and eigenenergies $\mathcal{E}_{\tau,\Lambda}^p$ depend parametrically on the hyperradius ρ_ξ . They are needed at a set of ρ values $\{\rho_\xi\}, \xi = 1, 2, \dots, n_\rho$, and are used as adiabatic basis functions for expanding the full wavefunction in each sector where $(\rho_\xi + \rho_{\xi-1})/2 \leq \rho \leq (\rho_{\xi+1} + \rho_\xi)/2$ for sector ξ . As shown elsewhere[9] this adiabatic-by-sector (or sector-Adiabatic) expansion of the wavefunction gives

rise to a set of coupled second order differential equations. These Coupled-Channel (CC) equations must be numerically integrated from a small value of the hyperradius ρ where the full wavefunction is zero to a large value of the hyperradius where asymptotic boundary conditions are applied. The term, $15\hbar^2/8\mu\rho_\xi^2$, in Eq. (19) results from removing the first derivative terms from the coupled channel (CC) equations; it is a constant in this equation and can be folded into the $\mathcal{E}_{\tau,\Lambda}^p$ if desired. In the numerical calculations we use atomic units throughout and therefore $\hbar = 1$. The quantity μ is the three-body reduced mass of the system arising from using mass-scaled coordinates. The three quantum numbers (Λ, p, τ) labeling $\mathcal{E}_{\tau,\Lambda}^p$ and $\Phi_{\tau,\Lambda}^p$ are: Λ is the component of the total angular momentum along the APH body-frame (BF) z -axis (the axis of least inertia of the three-body system), p is the parity quantum number with $p = 0$ or 1 , the parity of $\Phi_{\tau,\Lambda}^p$ under the parity transformation $\chi \rightarrow \chi \pm \pi$ is $(-1)^p$, and $\tau = 1, 2, \dots, n_\Phi$, which indexes the solutions in order of increasing energy.

Equation Eq. (19) differs from equation (164) of Reference[9] slightly because it omits a rotational term of the form $\frac{1}{2}(A + B)\hbar^2[J(J + 1) - \Lambda^2]$ as mentioned above. As pointed out by Launay and LeDourneuf [8], this gives surface functions $\Phi_{\tau,\Lambda}^p$ which are independent of the total angular momentum J , so many fewer surface functions must be calculated. The omitted term is easily included in the CC equations along with the remaining Coriolis and asymmetric top terms. This surface function basis is expected to produce rapid convergence of the CC expansion to the exact solution provided triangular symmetric top ($\theta = 0$) configurations are unimportant, which is the case for many reactions.

The full wavefunction must be continuous and regular everywhere. This requires that $\Phi_{\tau,\Lambda}^p$ must also be a continuous function of χ at $-\pi$ and π and regular everywhere. For systems with two or three identical atoms, the surface functions have other symmetries in addition to the parity, p , already defined and these symmetries will be exploited. The surface functions are real and normalized according to

$$\int_{-\pi}^{\pi} d\chi \int_0^{\pi/2} \Phi_{\tau',\Lambda}^{p'}(\theta, \chi; \rho_\xi) \Phi_{\tau,\Lambda}^p(\theta, \chi; \rho_\xi) \sin 2\theta d\theta = \delta_{\tau'\tau} \delta_{p'p}. \quad (21)$$

We now define

$$H_\theta = -\frac{4}{\sin 2\theta} \frac{\partial}{\partial \theta} \sin 2\theta \frac{\partial}{\partial \theta} \quad (22)$$

$$H_\chi = -\frac{\partial^2}{\partial \chi^2} \quad (23)$$

$$H_V = \frac{15\hbar^2}{8\mu\rho_\xi^2} + C\hbar^2\Lambda^2 + V(\rho_\xi, \theta, \chi) \quad (24)$$

so that the surface function Hamiltonian, Eq. (19), is

$$H = \frac{\hbar^2}{2\mu\rho_\xi^2} \left[H_\theta + \frac{1}{\sin^2 \theta} H_\chi \right] + H_V. \quad (25)$$

The discretized Hamiltonian is a matrix operator. In the rest of this paper, we use the term Hamiltonian to refer to this matrix.

3.2 Symmetrization of APH Hamiltonian

The Hamiltonian H in Eq. (25) is real but it is not symmetric, because H_θ is not symmetric. Therefore, if we use this form, we have to solve a non-symmetric matrix eigensystem requiring a large amount of memory and CPU time. It is therefore critical in the computation of APH surface functions to symmetrize H . The matrix H_θ is the non-symmetric part of H , and it is not periodic. We first extend H_θ to a periodic form and symmetrize it. Then the result is extended to symmetrize H .

Although H_θ is defined initially on $0 \leq \theta \leq \frac{\pi}{2}$, we note that it is invariant under the transformation $\theta \rightarrow \pi - \theta$ and hence we can expand the domain of $\psi(\theta)$ to the full real space by defining,

$$\psi(\theta) = \psi(\pi - \theta), \quad \frac{\pi}{2} \leq \theta \leq \pi \quad (26)$$

$$\psi(\theta + k\pi) = \psi(\theta), \quad 0 \leq \theta \leq \pi \text{ and } k = 0, \pm 1, \pm 2, \dots \quad (27)$$

Now $\psi(\theta)$ is a periodic function with a periodicity of π . Note that

$$H_\theta(\theta) = H(\pi - \theta) \quad (28)$$

$$H_\theta(\theta + k\pi) = H(\theta), \quad k = 0, \pm 1, \pm 2, \dots \quad (29)$$

One can see that the extended $\psi(\theta)$ satisfies $H_\theta\psi(\theta) = \lambda\psi(\theta)$ for any θ , i.e. the domain of H_θ is also extended to the full real space although it keeps its original form.

We comment that similar expressions for H_θ were obtained in Ref. [25] by using a symmetry adaptation procedure, wherein H_θ was projected on the right side onto a function belonging to the A_1 irreducible representation of the point group C_{2v} , and on the left side onto a function belonging to the A_2 irreducible representation of the point group C_{2v} . The choice of the A_1 irreducible representation conforms with the symmetry requirements presented in Eqs. Eq. (26) and Eq. (27) above. The A_2 irreducible representation was chosen due to the fact that the first derivative of an A_1 function is an A_2 function in C_{2v} . The resultant representation for H_θ in Ref. [25] is, however, not symmetric.

Here, to obtain a symmetric representation for H_θ , we transform it in two steps. First we introduce a continuous mapping function,

$$\theta(\gamma) = \frac{\pi}{4}[1 - \cos(\gamma + 2k\pi)] - k\pi, \quad k = 0, \pm 1, \pm 2, \dots \quad (30)$$

We note that the first derivative of this mapping is also continuous, but its second derivative is discontinuous at $\theta = k\pi/2$. This problem is handled by the mapping function itself: if we use a uniform grid for γ , it is equivalent to using a non-uniform grid for θ which is dense near the singularities ($\theta = k\pi/2$) and sparse otherwise, as shown in Fig. 2. Since more grid points are used in the $\theta = k\pi/2$ region, high accuracy can be obtained despite the discontinuity.

Substituting θ with γ in Eq. (22), we obtain,

$$H_\theta(\gamma) = -\frac{64}{\pi^2} \frac{1}{\sin 2\theta(\gamma) \sin \gamma} \frac{\partial \sin 2\theta(\gamma)}{\partial \gamma} \frac{\partial}{\sin \gamma} \frac{\partial}{\partial \gamma} \quad (31)$$

$H_\theta(\gamma)$ is very similar to $H_\theta(\theta)$ except that it has a periodicity of 2π .

In the second step, we define the transformation function

$$T = \sqrt{\sin 2\theta \sin \gamma} \quad (32)$$

We also observe that

$$T^\dagger = T \quad (33)$$

$$T^{-1} = \frac{1}{\sqrt{\sin 2\theta \sin \gamma}} \quad (34)$$

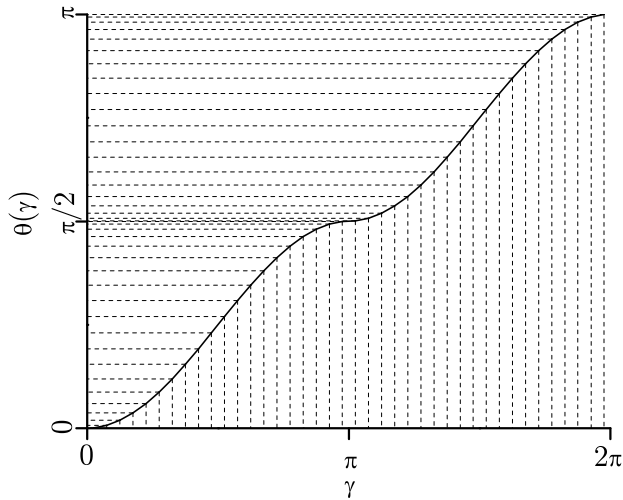


Figure 2: Grid mapping function $\theta(\gamma)$. The uniform grid in θ corresponds to the non-uniform grid for γ which is dense near the singularities ($\theta = k\pi/2$) and sparse otherwise.

and it is important to note that the singularities in T^{-1} are avoided by our choice of quadrature (see Sec. 2).

Applying T^\dagger to $H_\theta\psi(\theta) = \lambda\psi(\theta)$ and inserting the identity $T^{-1}T$ between H_θ and $\psi(\theta)$, we obtain

$$H_\gamma T\psi(\theta) = \lambda T\psi(\theta) \quad (35)$$

where

$$\begin{aligned} H_\gamma &= T^\dagger H_\theta(\gamma) T^{-1} \\ &= -\frac{64}{\pi^2} \frac{1}{\sqrt{\sin 2\theta(\gamma) \sin \gamma}} \frac{\partial \sin 2\theta(\gamma)}{\partial \gamma} \frac{\partial}{\sin \gamma} \frac{\partial}{\partial \gamma} \frac{1}{\sqrt{\sin 2\theta(\gamma) \sin \gamma}} \end{aligned} \quad (36)$$

is a symmetric Hamiltonian.

The eigenfunction of H_γ is

$$\tilde{\psi}(\gamma) = T(\gamma)\psi(\theta(\gamma)) \quad (37)$$

which is always zero at $\gamma = 0, \pi$, or 2π . It is not hard to see that extending $\psi(\theta)$ from $0 \leq \theta \leq \frac{\pi}{2}$ to $0 \leq \theta \leq \pi$ introduces undesired degenerate eigenvalues. If we reduce matrix H_γ from $0 \leq \theta \leq 2\pi$ to range $0 \leq \theta \leq \pi$ using the symmetry of ψ , we can eliminate those undesired degenerate eigenvalues. We use a grid similar to

the one used for PDAF;

$$\gamma_j = (j - \frac{1}{2})\Delta\gamma, \quad j = 1, 2N_\gamma \quad (38)$$

where $2N_\gamma$ is the number of grid points, and $\Delta\gamma = \frac{2\pi}{2N_\gamma} = \frac{\pi}{N_\gamma}$ is the distance between two consecutive grid points. For simplicity, we use a subscript j to denote a term evaluated at γ_j , and we also define the following terms,

$$t_j = \frac{1}{\sqrt{\sin 2\theta(\gamma_j) \sin \gamma_j}} \quad (39)$$

$$s_j = \frac{\sin 2\theta(\gamma_j)}{\sin \gamma_j} \quad (40)$$

Applying the derivative operator $D^{(1)}$ in Eq. (17) (substituting x with γ), the eigen-equation Eq. (35) can be written as

$$\begin{aligned} \lambda \tilde{\psi}_i &= \sum_{j=1}^{2N} \sum_{k=1}^{2N} -\frac{64}{\pi^2} t_i D_{ik}^{(1)} s_k D_{kj}^{(1)} t_j \tilde{\psi}_j \\ &= \left(\sum_{j=1}^N + \sum_{j=N+1}^{2N} \right) \sum_{k=1}^{2N} -\frac{64}{\pi^2} t_i D_{ik}^{(1)} s_k D_{kj}^{(1)} t_j \tilde{\psi}_j \\ &= \sum_{j=1}^N \sum_{k=1}^{2N} -\frac{64}{\pi^2} t_i D_{ik}^{(1)} s_k (D_{kj}^{(1)} + D_{k, 2N-j+1}^{(1)}) t_j \tilde{\psi}_j \\ &= \sum_{j=1}^N H_{\gamma_{ij}}^r \tilde{\psi}_j \end{aligned} \quad (41)$$

where

$$H_{\gamma_{ij}}^r = \sum_{k=1}^{2N} -\frac{64}{\pi^2} t_i D_{ik}^{(1)} s_k (D_{kj}^{(1)} + D_{k, 2N-j+1}^{(1)}) t_j \quad (42)$$

In the above derivation, $\tilde{\psi}_j = \tilde{\psi}_{2N-j+1}$, $t_j = t_{2N-j+1}$, $s_j = s_{2N-j+1}$ and the periodicity of $D^{(1)}$ is employed. One should note that in Eq. (41) $1 \leq i \leq N_\gamma$ and $1 \leq j \leq N_\gamma$, which means $0 \leq \gamma \leq \pi$, so H_γ^r is reduced to the original domain. H_γ^r is the desired symmetric matrix form for H_θ . It is, however, interesting to note that the bracketed quantity, $(D_{kj}^{(1)} + D_{k, 2N-j+1}^{(1)})$, in Eq. (42) is not an anti-symmetric matrix, in contrast to Ref. [25]. The full H_γ^r presented in Eq. (42) is symmetric by construction.

Similarly we can transform and discretize H to obtain its symmetric form. Using Eq. (25) the Schrödinger equation Eq. (18) reads

$$\left\{ \frac{\hbar^2}{2\mu\rho_\xi^2} \left[H_\theta + \frac{1}{\sin^2 \theta} H_\chi \right] + H_V \right\} \Phi_{\tau\Lambda}^p(\theta, \chi; \rho_\xi) = \mathcal{E}_{\tau\Lambda}^p(\rho_\xi) \Phi_{\tau\Lambda}^p(\theta, \chi; \rho_\xi) \quad (43)$$

We multiply by T^\dagger from the left on both sides of the above equation, and insert the identity $T^{-1}T$, to obtain

$$H^s \overline{\Phi}_{\tau\Lambda}^p(\theta, \chi; \rho_\xi) = \mathcal{E}_{\tau\Lambda}^p(\rho_\xi) \overline{\Phi}_{\tau\Lambda}^p(\theta, \chi; \rho_\xi) \quad (44)$$

where

$$H^s = \frac{\hbar^2}{2\mu\rho_\xi^2} \left[H_\gamma^r + \frac{1}{\sin^2\theta} H_\chi \right] + H_V \quad (45)$$

and

$$\overline{\Phi}_{\tau\Lambda}^p(\gamma, \chi; \rho_\xi) = T \Phi_{\tau\Lambda}^p(\theta, \chi; \rho_\xi) \quad (46)$$

The independence of the variables γ (or θ) and χ is used in the derivation. After discretization of the APH Hamiltonian, H^s is symmetric, because H_γ^r is symmetric, H_V is diagonal, and H_χ is obviously symmetric.

3.3 Reduction of the H_χ using point group symmetry

If the Hamiltonian H^s of a system commutes with a point group G , i.e. the potential H_V is symmetric under the operations of G , we can reduce the size of the Hamiltonian matrix by transforming the Hamiltonian into the irreducible representations of G .

Let $G = \{R\}$, where $\{R\}$ is a set of symmetry operations such as rotations and reflections. The order of G is h , i.e. G contains h symmetry operations, R . Suppose H_χ satisfies the following eigen-equation,

$$H_\chi \phi^{[z,\kappa]}(\chi) = \lambda \phi^{[z,\kappa]}(\chi) \quad (47)$$

where $\phi^{[z,\kappa]}$ transform according the κ -th column of the z -th irreducible representation of G , i.e. $\phi^{[z,\kappa]}$ is the κ -th basis function for the z -th irreducible representation, and λ is the corresponding eigenvalue. We will discretize Eq. (47) using a uniform grid

$$\chi_j = (j - 1/2)\Delta\chi, \quad j = 1, hN_\chi \quad (48)$$

where hN_χ is the number of grid points, $\Delta\chi = \frac{2\pi}{hN_\chi}$ is the spacing between consecutive grid points, and clearly N_χ is the number of grid points in interval $[0, \frac{2\pi}{h}]$. Then Eq. (47) can be written as,

$$\sum_{j=1}^{hN_\chi} H_\chi(\chi_i, \chi_j) \phi^{[z,\kappa]}(\chi_j) = \lambda \phi^{[z,\kappa]}(\chi_i), \quad \kappa = 1, \{l_z\} \quad (49)$$

where l_z is the dimension of the z -th irreducible representation. The full range of χ can be generated by

applying each symmetry operation R on the range $[1, N\chi]$. We can then write Eq. (49) as

$$\sum_{j=1}^{N\chi} \sum_R H_\chi(\chi_i, R\chi_j) \phi^{[z,\kappa]}(R\chi_j) = \lambda \phi^{[z,\kappa]}(\chi_i), \quad \kappa = 1, \{l_z\} \quad (50)$$

From the well-known relations [30],

$$\phi^{[z,\kappa]}(R^{-1}\chi) = \sum_{\kappa'} \phi^{[z,\kappa']}(\chi) \Gamma_{\kappa',\kappa}^{[z]}(R) \quad (51)$$

where $\Gamma_{\kappa',\kappa}^{[z]}(R)$ is the (κ', κ) -th element of the z -th irreducible representation matrix of R , we have,

$$\begin{aligned} \phi^{[z,\kappa]}(R\chi) &= \sum_{\kappa'} \phi^{[z,\kappa']}(\chi) \Gamma_{\kappa',\kappa}^{[z]}(R^{-1}) \\ &= \sum_{\kappa'} \phi^{[z,\kappa']}(\chi) \Gamma_{\kappa',\kappa}^{[z]\dagger}(R) \\ &= \sum_{\kappa'} \phi^{[z,\kappa']}(\chi) \Gamma_{\kappa,\kappa'}^{[z]*}(R) \end{aligned} \quad (52)$$

The following obvious properties of $\Gamma_{\kappa',\kappa}^{[z]}(R)$ are used in the above derivation,

$$\Gamma^{[z]}(R^{-1}) = \Gamma^{[z]\dagger}(R) = \Gamma^{[z]-1}(R) \quad (53)$$

Substituting Eq. (52) into Eq. (50), we obtain,

$$\sum_{j=1}^{N\chi} \sum_R H_\chi(\chi_i, R\chi_j) \sum_{\kappa'} \phi^{[z,\kappa']}(\chi_j) \Gamma_{\kappa,\kappa'}^{[z]*}(R) = \lambda \phi^{[z,\kappa]}(\chi_i), \quad \kappa = 1, \{l_z\} \quad (54)$$

The expression Eq. (54) is a set of coupled equations which can be written concisely in a matrix form. For triatomic reactions, the relevant irreducible representations are either one-dimensional or two-dimensional. For the one-dimensional case, $\kappa = \kappa' = 1$, so we simply omit them. Hence we have,

$$\sum_{j=1}^{N\chi} H_\chi^r(\chi_i, \chi_j) \phi^{[z]}(\chi_j) = \lambda \phi^{[z]}(\chi_i) \quad (55)$$

where

$$H_\chi^r(\chi_i, \chi_j) = \sum_R H_\chi(\chi_i, R\chi_j) \Gamma^{[z]*}(R) \quad (56)$$

is the reduced H_χ in a one-dimensional irreducible representation.

For the two-dimensional case, we have,

$$\sum_{j=1}^{N_\chi} H_\chi^r(\chi_i, \chi_j) \begin{pmatrix} \phi^{[z,1]}(\chi_j) \\ \phi^{[z,2]}(\chi_j) \end{pmatrix} = \lambda \begin{pmatrix} \phi^{[z,1]}(\chi_i) \\ \phi^{[z,2]}(\chi_i) \end{pmatrix} \quad (57)$$

where

$$H_\chi^r(\chi_i, \chi_j) = \sum_R H_\chi(\chi_i, R\chi_j) \Gamma^{[z]^*}(R) \quad (58)$$

is the reduced H_χ in a two-dimensional irreducible representation. It has the same form as in the one-dimensional case, but it is a 2×2 matrix. H_χ^r can be proved to be symmetric if the associated irreducible representation matrices are real (see Appendix **A**). There are three types of triatomic interactions:

ABC All atoms are distinct. The point group corresponding to this type is C_2

AAB Two atoms are identical. The point group corresponding to this type is C_{2v}

AAA All atoms are identical. The point group corresponding to this type is C_{6v}

For all the above groups in each type, the irreducible representation matrices are all real, so H_χ^r is symmetric.

We provide the representation matrices in Appendix **B** for convenience.

One should note that if we confine χ to $[0, \frac{2\pi}{h}]$, H_χ^r is a $N_\chi \times N_\chi$ matrix in an one-dimensional irreducible representation and a $2N_\chi \times 2N_\chi$ matrix in a two-dimensional irreducible representation. When the eigen-system of Eq. (55) or Eq. (57) is solved, eigenfunctions in the range $[0, \frac{2\pi}{h}]$ are obtained. One can employ Eq. (51) to compute the eigenfunctions on the full range of χ .

One can see that using H_χ^r instead of H_χ doesn't affect the symmetrization of H in Sec. 3.2. Hence we shall use the following definition of H^s in the rest of this paper

$$H^s = \frac{\hbar^2}{2\mu\rho_\xi^2} \left[H_\gamma^r + \frac{1}{\sin^2\theta} H_\chi^r \right] + H_V \quad (59)$$

The derivation presented here may be contrasted with the symmetry-adaptation procedure provided in Ref. [25]. In Ref. [25] the symmetry-adaptation was carried out by projection of the Hamiltonian (or the derivative operator) onto two different sets of projectors, one on each side of the Hamiltonian matrix. This is useful for cases where the Hamiltonian (or the derivative operator) changes the symmetry of the function it acts on (for example, as in the case of the d/dx operator). In the present case, the symmetry-adaptation introduced in this section is only used to adapt the χ -part of the Hamiltonian, which is totally symmetric

and hence does not change the symmetry of the functions it acts on (unlike the operator corresponding to the θ -part).

3.4 Reduction of the Hamiltonian using projection

Suppose we discretize H^s using N_χ grid points in χ coordinate and N_γ in γ . The size of the Hamiltonian matrix ($N_\gamma N_\chi \times N_\gamma N_\chi$) to be diagonalized is very large for systems of physical interest when highly accurate eigenvalues and eigenfunctions are needed. Since we wish to obtain only a few of the lowest eigenstates to high accuracy, we consider here a projection technique to reduce the size of the Hamiltonian matrix, which leads to reduction in the CPU time and memory requirements. First we find a nearly complete basis for the desired lowest eigenvectors, and then we project the Hamiltonian matrix to this basis: $H^{\text{cut}} = \tilde{P}H^sP$, where P is the projection matrix and \tilde{P} is the transpose of P . The matrix H^{cut} is small. We solve the eigensystem of H^{cut} and map it back to the original basis to obtain the approximate eigensystem of the H . Details are given below.

Noting that H_γ^r depends only on γ and $\frac{\hbar^2}{2\mu\rho_\xi^2}$ is a constant, and introducing the identity matrices I_γ and I_χ in the γ and χ spaces respectively, we can rewrite the Hamiltonian H^s in Eq. (59) in the tensor product form,

$$H^s = \frac{\hbar^2}{2\mu\rho_\xi^2}H_\gamma^r \otimes I_\chi + \left(\frac{\hbar^2}{2\mu\rho_\xi^2}\frac{1}{\sin^2\theta}I_\gamma \otimes H_\chi^r + H_V I_\gamma \otimes I_\chi\right) \quad (60)$$

Now H^s is divided into two terms

$$H_1^s = \frac{\hbar^2}{2\mu\rho_\xi^2}H_\gamma \otimes I_\chi \quad (61)$$

$$H_2^s = \frac{\hbar^2}{2\mu\rho_\xi^2}\frac{1}{\sin^2\theta}I_\gamma \otimes H_\chi + H_V I_\gamma \otimes I_\chi \quad (62)$$

The first term, H_1^s , is independent of χ , while the second term depends on both γ and χ . Since we are only interested in the lowest eigenvalues and eigenfunctions of H^s , and H_1^s is independent of χ , we can expect to get accurate results using only a subeigenspace of H_2^s instead. We solve the eigensystem of H_2^s for each fixed γ_j ,

$$H_2^s(\gamma_j)\alpha_k^{\gamma_j} = \lambda_k^{\gamma_j}\alpha_k^{\gamma_j} \quad j = 1, N_\gamma \quad (63)$$

where N_γ is the number of the grid points used in γ and $(\lambda_k^{\gamma_j}, \alpha_k^{\gamma_j})$ is the k -th eigenpair for the given γ_j . Then we discard the eigenvectors with large eigenvalues. The rest of the eigenvectors consist of a nearly complete

basis for the lowest eigenvectors of H^s . In our implementation, we sort all the eigenvectors obtained above in ascending order of eigenvalues, and choose only a number of the eigenvectors corresponding to the smallest eigenvalues. After normalization we construct the projection matrix,

$$P = \begin{pmatrix} P_1 & & & \\ & P_2 & & \\ & & \ddots & \\ & & & P_{N_\gamma} \end{pmatrix} \quad (64)$$

where

$$P_i = (\alpha_1^{\gamma_i}, \alpha_2^{\gamma_i}, \dots, \alpha_{m_{\gamma_i}}^{\gamma_i}) \quad (65)$$

Because P is an orthonormal, nearly complete basis for the lowest eigenvectors, $\overline{\Phi}_{\tau\Lambda}^p(\gamma, \chi; \rho_\xi)$, we have

$$P\tilde{P}\overline{\Phi}_{\tau\Lambda}^p(\gamma, \chi; \rho_\xi) \approx \overline{\Phi}_{\tau\Lambda}^p(\gamma, \chi; \rho_\xi) \quad (66)$$

Substituting $\overline{\Phi}_{\tau\Lambda}^p(\gamma, \chi; \rho_\xi)$ in Eq. (44) and multiplying by \tilde{P} from the left we get,

$$H^{\text{cut}}\Psi_{\tau\Lambda}^p(\gamma, \chi; \rho_\xi) \approx \mathcal{E}_{\tau\Lambda}^p(\rho_\xi)\Psi_{\tau\Lambda}^p(\gamma, \chi; \rho_\xi) \quad (67)$$

where

$$H^{\text{cut}} = \tilde{P}HP \quad (68)$$

and

$$\Psi_{\tau\Lambda}^p(\gamma, \chi; \rho_\xi) = \tilde{P}\overline{\Phi}_{\tau\Lambda}^p(\gamma, \chi; \rho_\xi) \quad (69)$$

We can see that P is a $N_\gamma N_\chi \times N_\chi^{\text{cut}}$ matrix, where

$$N^{\text{cut}} = \sum_{i=1}^{N_\gamma} m_{\gamma_i} \quad (70)$$

so H^{cut} is a $N^{\text{cut}} \times N^{\text{cut}}$ matrix. Its size is much smaller than the size of H^s if N^{cut} is much smaller than $N_\gamma N_\chi$, which is the case if we want only a few eigenvalues. N^{cut} should be taken to be as small as possible, consistent with the desired level of convergence.

Noting that H^s is symmetric, we have

$$\tilde{H}^{\text{cut}} = \tilde{P}\tilde{H}^sP = \tilde{P}H^sP = H^{\text{cut}} \quad (71)$$

Thus H^{cut} is symmetric.

4 Numerical Tests

Numerical tests are carried out to study three aspects of the approach. First, we test the behavior with respect to parameter M in the PDAF $\delta_{p,M}^{(k)}$. Next we examine the H_χ^r using different irreducible representations of various groups. Finally, the accuracy of H_γ^r is tested.

4.1 Test of PDAFs

We tested PDAFs using different periodic functions, all of them showing similar results. Here we present only the test for the eigenvalues of H_χ . Using the PDAF matrix defined in Eq. (17), we obtain the discrete representation of H_χ ,

$$\begin{aligned} H_{\chi ij} &= -\sum_{k=1}^{N_\chi} D_{ij}^{(2)} \\ &= -\sum_{k=1}^{N_\chi} \delta_{p,M}^{(2)}(\chi_i - \chi_j)\Delta\chi \end{aligned} \quad (72)$$

where N_χ is the number of grid points used in $(0, 2\pi)$, $\Delta\chi = 2\pi/N_\chi$ and $\chi_j = (j - \frac{1}{2})\Delta\chi$. We know that the correct eigenvalues of H_χ should be $0, 1, 1, 4, 4, \dots, k^2, k^2, \dots$, so it's easy to check the difference between the computed eigenvalues and the exact ones. We set the criteria of 10^{-6} as the maximum tolerable error and then count how many good eigenvalues can be obtained. A typical result is shown in Fig. 3, in which we set $N_\chi = 32$ and various M from 1 to 35. One can see that when $M = N_\chi/2$, almost all eigenvalues are good. This suggests the optimal choice of M .

4.2 Test of H_χ^r

Tests of H_χ^r were done for all the aforementioned irreducible representations of the relevant point groups. All of them give good results. Here we present only one typical result computed using the C_{2v} group, since only C_{2v} is involved in the FH_2 reaction calculation.

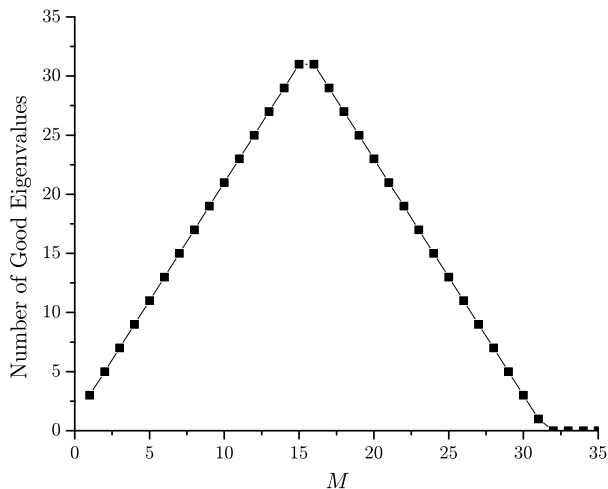


Figure 3: The number of good eigenvalues reaches maximum when $M = N_\chi/2$ ($N_\chi = 32$), where M is the parameter in PDAF $\delta_{p,M}^{(k)}(x)$, and N_χ is the number of grid points in range $(0, 2\pi)$.

Similar to H_χ , we can obtain the PDAF representation of H_χ^r . Note that C_{2v} has only one-dimensional irreducible representations, so we use Eq. (56) for H_χ^r . We obtain the discrete representation of H_χ^r as,

$$H_{\chi_{ij}} = - \sum_{k=1}^{N_\chi} \sum_R \delta_{p,M}^{(2)}(\chi_i - R\chi_j) \Gamma^{[z]} \Delta\chi \quad (73)$$

Note that the grid scheme is defined in Eq. (48). We set $N_\chi = 8$, and the eigenvalues λ_k for each of the irreducible representations are computed, and the $\sqrt{\lambda_k}$ are shown in table Tbl. 1 for easy comparison. One can see that if we combine the results from all the irreducible representations, we will obtain the (approximate) eigenvalues $0, 1, 1, 4, 4, \dots, k^2, k^2, \dots$, which are obtained from H_χ . We also note that the degenerate eigenvalues in H_χ are no longer degenerate in H_χ^r .

k	A_1	B_1	A_2	B_2
1	0.00000052456066	2.00000000000009	0.99999999999989	1.00000000000007
2	2.00000000000007	3.99999999999997	3.00000000000004	3.00000000000002
3	3.99999999999999	5.99999999999999	5.00000000000000	5.00000000000000
4	5.99999999999999	7.99999999999999	7.00000000000000	7.00000000000000
5	7.99999999999999	10.00000000000000	9.00000000000001	9.00000000000001
6	10.00000000000000	12.00000000000000	11.00000000000000	11.00000000000000
7	12.00000000000000	14.00000000000000	13.00000000000000	13.00000000000000
8	14.00000000000000	22.6274169979695	15.00000000000000	15.00000000000000

Table 1: $\sqrt{\lambda_k}$, square roots of eigenvalues of H_χ^r in irreducible representations of group C_{2v}

4.3 Test of H_γ^r

H_γ^r in Eq. (42) has the same eigenvalues as H_θ in Eq. (22). If we rewrite H_θ as

$$H_\theta = -\frac{8}{\sin 2\theta} \frac{\partial}{\partial 2\theta} \sin 2\theta \frac{\partial}{\partial 2\theta} \quad (74)$$

we can see that the eigen-equation of $H_\theta\psi(\theta) = \lambda\psi(\theta)$, is a Legendre differential equation if we write the eigenvalue as

$$\lambda_l = 8l(l+1) \quad l = 0, 1, \dots \quad (75)$$

Thus H_γ^r has eigenvalues of $8l(l+1)$. To evaluate the accuracy of the computed eigenvalue, we define $S_l(\lambda_l)$ as follows,

$$S_l(\lambda_l) = \begin{cases} -\lg |\lambda_l| & l=0, \\ -\lg \frac{\lambda_l - 8l(l+1)}{8l(l+1)} & l > 0 \end{cases} \quad (76)$$

where λ_l is the l -th computed eigenvalue, and $S_l(\lambda_l)$ gives the approximate number of significant digits. Fig. 4 shows the results when we set $N_\gamma = 16, 32, 48$ and 64 . One can see that for each N_γ there are about $N_\gamma/3$ eigenvalues of high accuracy. This is accurate enough for the FH_2 calculation, because typically the order of the Hamiltonian matrix is about 1000 but we require less than 300 eigenvalues.

It is worth mentioning that we also tested the non-symmetric form, H_θ , using the PDAF presentation. Although we can get as highly accurate results as we get from H_χ or H_χ^r , we still choose the symmetric form, because the non-symmetric matrix costs more time and memory to diagonalize. Moreover, when we add the potential, the accuracy of the non-symmetric form will decrease to the accuracy of the symmetric H_γ^r .

5 Calculations for the FH_2 System

In this section we report the results of PDAF calculations of surface functions and the matrix elements, and compare them with the results of the DVR and ABM methods. The system chosen as a nontrivial example is the $F+H_2 \rightarrow HF+H$ reaction; its treatment requires generation of a large basis of surface functions. The potential energy surface (PES) used is that of Brown *et al.*[29] commonly called the T5A surface, and we choose the zero of energy to be at the bottom of the asymptotic HF potential wells. This PES has been used in many calculations[8, 28, 14, 20, 31, 32, 33] on this reaction, and plots of the PES and surface functions showing their appearance in APH coordinates have also been published. Arrangement 1 or i(initial) is taken to be $F+H_2$ reactants.

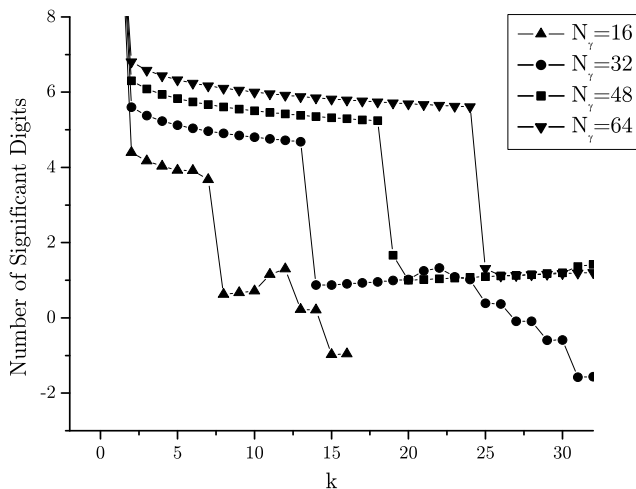


Figure 4: Accuracy (number of significant digits) in eigenvalues of H_γ^r . For all N_γ , the smallest $N_\gamma/3$ eigenvalues are of high accuracy.

The calculations are for $\Lambda = 0$ and even parity ($p = 0$) and include all functions connecting to the even j rotational states of the $F+H_2$ arrangement. Because of the symmetry due to the identical H atoms, this only requires including in the PDAF calculations the A_1 irreducible representation, in which the surface functions are even under reflection about $\chi = 0$.

5.1 Grid Size and Mapping

The grid sizes (the number of grid points), N_χ , N_γ , and N^{cut} are determined by the convergence test. We present only the results here. To attain five significant digits in the lowest 100 eigenvalues for any ρ_ξ ,

$$N_\gamma = \lfloor 25.852 + 5.85119\rho_\xi - 0.130102\rho_\xi^2 - 0.0042517 * \rho_\xi^3 \rfloor \quad (77)$$

$$N^{\text{cut}} = \lfloor 1428.06 + 29.2007\rho_\xi - 6.37755\rho_\xi^2 - 0.119048 * \rho_\xi^3 \rfloor \quad (78)$$

$$N_\chi = \lfloor 4\pi \max(N_\gamma) \rfloor / h \quad (79)$$

where h is the order of the associated symmetry group. To get N_χ , we use the maximum of N_γ because it makes N_χ identical for all ρ_ξ , thus making it easy to compute the overlap matrices. Also, using the maximum

N_γ doesn't significantly increase the computation time, because we reduce the matrix size according to N^{cut} , as discussed in Sec. 3.4.

Although N_χ is chosen to be the same for all ρ_ξ , N_γ is different. Hence, before we compute the overlap matrix, we have to map the wave functions to a uniform grid, to reduce the computation time for the overlap matrix.

Let N_γ^u be the number of uniform grid points in γ ; N_γ is the original number of grid points. Applying Eq. (15) to the wave function

$$\begin{aligned}
\Phi_{\tau\Lambda}^p(\gamma_j, \chi; \rho_\xi) &= \sum_{k=1}^{2N_\gamma} \delta_{p,M}(\gamma_j - \gamma_k) \Phi_{\tau\Lambda}^p(\gamma_k, \chi; \rho_\xi) \Delta\gamma \\
&= \sum_{k=1}^{N_\gamma} \{ \delta_{p,M}(\gamma_j - \gamma_k) \Phi_{\tau\Lambda}^p(\gamma_k, \chi; \rho_\xi) + \delta_{p,M}(\gamma_j - 2\pi + \gamma_k) \Phi_{\tau\Lambda}^p(2\pi - \gamma_k, \chi; \rho_\xi) \} \Delta\gamma \\
&= \sum_{k=1}^{N_\gamma} [\delta_{p,M}(\gamma_j - \gamma_k) + \delta_{p,M}(\gamma_j - 2\pi + \gamma_k)] \Phi_{\tau\Lambda}^p(\gamma_k, \chi; \rho_\xi) \Delta\gamma
\end{aligned} \tag{80}$$

where $\Delta\gamma = \pi/N_\gamma$, and γ_j, γ_k represent the coordinates in the above two grid schemes respectively,

$$\gamma_j = (j - \frac{1}{2})\Delta\gamma^u \tag{81}$$

$$\gamma_k = (k - \frac{1}{2})\Delta\gamma \tag{82}$$

where $\Delta\gamma^u = \pi/N_\gamma^u$

5.2 Eigenvalues

The atomic masses used are:

$$\text{mass of F} = 18.9984032 \text{ a.u.} \tag{83}$$

$$\text{mass of H} = 1.00782503 \text{ a.u.} \tag{84}$$

The calculations were performed at five representative ρ values ranging from the smallest to the largest values that were needed in our reactive scattering calculations[14, 20]. The precise values of ρ chosen have no particular significance, and some were chosen simply because the convergence of the DVR method had

already been studied at these values.

The results are given in Tbl. 2 through Tbl. 6 for the five values of ρ chosen. In each table, the energy eigenvalues of the highest ten important or open surface function states are given in eV. The omitted lower eigenvalues always agree to more significant figures than those shown. Also shown is $\bar{\mathcal{E}}(n)$, the average of the first n eigenvalues. This gives a convenient measure of the overall agreement of the methods.

τ	PDAF	ABM	DVR	FEM
1	6.9176	6.9177	6.9177	6.9177
2	7.0341	7.0341	7.0341	7.0342
3	7.1299	7.1298	7.1296	7.1299
4	7.3044	7.3042	7.3038	7.3043
5	7.4934	7.4932	7.4927	7.4933
6	7.7007	7.7007	7.7008	7.7009
7	7.9227	7.9219	7.9202	7.9222
8	8.0786	8.0789	8.0786	8.0791
9	8.1548	8.1524	8.1475	8.1529
10	8.2495	8.2502	8.2494	8.2503
$\bar{\mathcal{E}}(10)$	7.5986	7.5983	7.5974	7.5985

Table 2: PDAF, ABM, DVR, and FEM surface function energies \mathcal{E}_τ and average energies in eV at $\rho = 2.2 a_0$.

τ	PDAF	ABM	DVR	FEM
11	1.9845	1.9845	1.9845	1.9849
12	1.9975	1.9975	1.9975	1.9979
13	2.0514	2.0515	2.0515	2.0519
14	2.1090	2.1090	2.1090	2.1093
15	2.1275	2.1275	2.1275	2.1281
16	2.1352	2.1352	2.1353	2.1357
17	2.1993	2.1994	2.1994	2.1998
18	2.2578	2.2578	2.2578	2.2584
19	2.2730	2.2730	2.2730	2.2737
20	2.3197	2.3197	2.3197	2.3204
$\bar{\mathcal{E}}(20)$	1.8551	1.8551	1.8551	1.8554

Table 3: PDAF, ABM, DVR, and FEM surface function energies \mathcal{E}_τ and average energies in eV at $\rho = 3.0375828 a_0$.

5.3 Matrix Elements

The APH surface functions $\Phi_{\tau\Lambda}^p(\gamma, \chi; \rho_\xi)$ are “sector adiabatic”; that is, they change from sector to sector, but are independent of ρ within a sector. Thus, when the APH wave function is substituted into the Schrödinger equation, the resulting exact coupled channel or close coupling equations are of the form[9]

τ	PDAF	ABM	DVR	FEM
91	2.0699	2.0701	2.0701	2.0720
92	2.0721	2.0734	2.0727	2.0760
93	2.0864	2.0896	2.0869	2.0916
94	2.0941	2.0941	2.0943	2.0961
95	2.1087	2.1107	2.1093	2.1132
96	2.1215	2.1232	2.1220	2.1267
97	2.1487	2.1509	2.1495	2.1549
98	2.1643	2.1650	2.1645	2.1672
99	2.1793	2.1806	2.1799	2.1833
100	2.1892	2.1892	2.1893	2.1918
$\bar{\mathcal{E}}(100)$	1.3974	1.3977	1.3975	1.3985

Table 4: PDAF, ABM, DVR, and FEM surface function energies \mathcal{E}_τ and average energies in eV at $\rho = 4.9747966 a_0$.

τ	PDAF	ABM	DVR	FEM
91	2.0559	2.0564	2.0569	2.0679
92	2.0749	2.0754	2.0760	2.0928
93	2.0980	2.0981	2.0981	2.1023
94	2.0985	2.0990	2.0994	2.1141
95	2.1098	2.1098	2.1099	2.1148
96	2.1194	2.1196	2.1198	2.1278
97	2.1268	2.1273	2.1278	2.1443
98	2.1538	2.1542	2.1543	2.1537
99	2.1551	2.1551	2.1551	2.1608
100	2.1597	2.1602	2.1608	2.1621
$\bar{\mathcal{E}}(100)$	1.3788	1.3788	1.3790	1.3811

Table 5: PDAF, ABM, DVR, and FEM surface function energies \mathcal{E}_τ and average energies in eV at $\rho = 7.2989993 a_0$.

τ	PDAF	ABM	DVR	FEM
91	2.0747	2.0747	2.0748	2.0805
92	2.0774	2.0779	2.0782	2.0863
93	2.0957	2.0964	2.0974	2.1051
94	2.1010	2.1010	2.1009	2.1065
95	2.1153	2.1153	2.1154	2.1233
96	2.1189	2.1194	2.1197	2.1284
97	2.1250	2.1252	2.1253	2.1315
98	2.1461	2.1470	2.1482	2.1541
99	2.1542	2.1545	2.1546	2.1562
100	2.1558	2.1559	2.1560	2.1564
$\bar{\mathcal{E}}(100)$	1.3791	1.3791	1.3792	1.3812

Table 6: PDAF, ABM, DVR, and FEM surface function energies \mathcal{E}_τ and average energies in eV at $\rho = 9.0a_0$.

$$\left[\frac{\partial^2}{\partial \rho^2} + \frac{2\mu E}{\hbar^2} \right] \psi_{\tau\Lambda}^{Jpn}(\rho) = \frac{2\mu}{\hbar^2} \sum_{\tau'A'} \langle \Phi_{\tau\Lambda}^{Jp} \hat{D}_{\Lambda M}^{Jp} | H_i | \Phi_{\tau'A'}^{Jp} \hat{D}_{\Lambda'M}^{Jp} \rangle \psi_{\tau'A'}^{Jpn}(\rho) \quad (85)$$

The matrix elements are obtained in Reference [9] as,

$$\begin{aligned} \langle \Phi_{\tau\Lambda}^{Jp} \hat{D}_{\Lambda M}^{Jp} | H_i | \Phi_{\tau'A'}^{Jp} \hat{D}_{\Lambda'M}^{Jp} \rangle &= \frac{\rho_\xi^2}{\rho^2} \mathcal{E}_{\tau\Lambda}(\rho_\xi) \delta_{\tau\tau'} \delta_{\Lambda\Lambda'} \\ &+ \delta_{\Lambda\Lambda'} \langle \Phi_{\tau\Lambda}^{Jp} \left| V(\rho, \theta, \chi) - \frac{\rho_\xi^2}{\rho^2} V(\rho_\xi, \theta, \chi) \right| \Phi_{\tau'A'}^{Jp} \rangle \\ &+ \langle \Phi_{\tau\Lambda}^{Jp} \hat{D}_{\Lambda M}^{Jp} \left| \frac{A-B}{2} (J_x^2 - J_y^2) + T_c \right| \Phi_{\tau'A'}^{Jp} \hat{D}_{\Lambda'M}^{Jp} \rangle \end{aligned} \quad (86)$$

where ρ_ξ denotes the ξ^{th} hyper-radius sampled from interval $[\rho_{\min}, \rho_{\max}]$. The ρ_ξ are given by

$$\rho_\xi = [\rho_{\min} + (\xi - 1)\Delta\rho_1](1 + \Delta\rho_2)^{\xi-1} \quad (87)$$

This algorithm spaces the sector centers logarithmically. Given a sector with sector center ρ_ξ , we evaluate matrix elements at the three rho values given by

$$\rho_1 = \frac{\rho_{\xi-1} + \rho_\xi}{2} \quad (88)$$

$$\rho_2 = \rho_\xi \quad (89)$$

$$\rho_3 = \frac{\rho_\xi + \rho_{\xi+1}}{2} \quad (90)$$

All the matrix elements in Eq. (86) are independent of E , so that they can be calculated once, stored, and used at many scattering energies.

The wave functions $\Phi_{\tau,\Lambda}^p(\gamma, \chi; \rho_\xi)$ should be normalized before computation of the matrix elements. The normalization factor N can be calculated in the desired irreducible representation easily according to Eq. (21) as shown below,

$$\begin{aligned}
1 &= N \int_0^{2\pi} d\chi \int_0^{\pi/2} d\theta \sin 2\theta \Phi_{\tau\Lambda}^{p,2}(\theta, \chi; \rho_\xi) \\
&= N \int_0^{2\pi} d\chi \int_0^\pi d\gamma \frac{\pi}{4} \sin \gamma \sin 2\theta \Phi_{\tau\Lambda}^{p,2}(\gamma, \chi; \rho_\xi) \\
&= N \sum_{i=1}^{hN_\chi} \sum_{j=1}^{N_\gamma} \Delta\chi \Delta\gamma \frac{\pi}{4} \sin \gamma_j \sin 2\theta(\gamma_j) \Phi_{\tau\Lambda}^{p,2}(\gamma_j, \chi_i; \rho_\xi) \\
&= N \sum_{i=1}^{N_\chi} \sum_{j=1}^{N_\gamma} \sum_R \Delta\chi \Delta\gamma \frac{\pi}{4} \sin \gamma_j \sin 2\theta(\gamma_j) \Phi_{\tau\Lambda}^p(\gamma_j, R^{-1}\chi_i; \rho_\xi) \Phi_{\tau\Lambda}^p(\gamma_j, R^{-1}\chi_i; \rho_\xi) \\
&= N \sum_{i=1}^{N_\chi} \sum_{j=1}^{N_\gamma} \sum_R \Delta\chi \Delta\gamma \frac{\pi}{4} \sin \gamma_j \sin 2\theta(\gamma_j) \Gamma^{[z]}(R) \Phi_{\tau\Lambda}^{p,2}(\gamma_j, \chi_i; \rho_\xi) \\
&= hN \sum_{i=1}^{N_\chi} \sum_{j=1}^{N_\gamma} \Delta\chi \Delta\gamma \frac{\pi}{4} \sin \gamma_j \sin 2\theta(\gamma_j) \Phi_{\tau\Lambda}^{p,2}(\gamma_j, \chi_i; \rho_\xi)
\end{aligned}$$

Thus

$$N = \left\{ \frac{1}{4} h\pi \Delta\chi \Delta\gamma \sum_{i=1}^{N_\chi} \sum_{j=1}^{N_\gamma} \sin \gamma_j \sin 2\theta(\gamma_j) \Phi_{\tau\Lambda}^{p,2}(\gamma_j, \chi_i; \rho_\xi) \right\}^{-\frac{1}{2}} \quad (91)$$

After $\Phi_{\tau\Lambda}^p(\gamma, \chi; \rho_\xi)$ is normalized, we compute the matrix elements. The first term on the right-hand side of Eq. (86) is just a local internal energy which together with the E -term on the left-hand side of Eq. (85) determines a local wave number.

The second term of Eq. (85) is often called a potential matrix element. It is small on the sector and can be evaluated with the same quadratures used in getting the surface functions. Similar to the evaluation of the normalization factor, we obtain for the potential matrix elements,

$$\begin{aligned}
\langle \Phi_{\tau\Lambda}^{Jp}(\rho_\xi) | V(\rho) - \frac{\rho_\xi^2}{\rho^2} V(\rho_\xi) | \Phi_{\tau'\Lambda}^{Jp}(\rho_\xi) \rangle &= \frac{1}{4} h\pi \Delta\chi \Delta\gamma \sum_{i=1}^{N_\chi} \sum_{j=1}^{N_\gamma} \sin \gamma_j \sin 2\theta(\gamma_j) \times \\
&\quad \Phi_{\tau\Lambda}^p(\gamma_j, \chi_i; \rho_\xi) \left[V(\rho) - \frac{\rho_\xi^2}{\rho^2} V(\rho_\xi) \right] \Phi_{\tau'\Lambda}^p(\gamma_j, \chi_i; \rho_\xi) \quad (92)
\end{aligned}$$

The Coriolis term can be simplified as

$$\begin{aligned}
\langle \Phi_{\tau\Lambda}^{Jp} \hat{D}_{\Lambda M}^{Jp} | T_c | \Phi_{\tau'\Lambda'}^{Jp} \hat{D}_{\Lambda' M}^{Jp} \rangle &= \frac{-\hbar^2}{2\mu\rho^2} \left\langle \Phi_{\tau\Lambda}^p \left| \frac{\cos\theta}{\sin^2\theta} \frac{\partial}{\partial\chi} \right| \Phi_{\tau'\Lambda'}^p \right\rangle \\
&\times [(1 + \delta_{\Lambda 0})(1 + \delta_{\Lambda' 0})]^{-1/2} \\
&\times [\lambda_+(J, \Lambda)\delta_{\Lambda', \Lambda+1} - \lambda_-(J, \Lambda)\delta_{\Lambda', \Lambda-1} \\
&+ \lambda_-(J, \Lambda)(-1)^{J+\Lambda+p}\delta_{\Lambda', 1-\Lambda}]
\end{aligned} \tag{93}$$

where

$$\lambda_{\pm}(J, \Lambda) = [(J \pm \Lambda + 1)(J \mp \Lambda)]^{\frac{1}{2}} \tag{94}$$

and

$$\begin{aligned}
\left\langle \Phi_{\tau\Lambda}^p \left| \frac{\cos\theta}{\sin^2\theta} \frac{\partial}{\partial\chi} \right| \Phi_{\tau'\Lambda'}^p \right\rangle &= \frac{1}{2} h\pi \Delta \chi^2 \Delta \gamma \sum_{i=1}^{N_x} \sum_{j=1}^{N_\gamma} \sum_{k=1}^{N_x} \sin \gamma_j \frac{\cos^2 \theta(\gamma_j)}{\sin \theta(\gamma_j)} \times \\
&\Phi_{\tau\Lambda}^p(\gamma_j, \chi_i; \rho_\xi) \delta_{p,M}^{(1)}(\chi_i - \chi_k) \Phi_{\tau'\Lambda'}^p(\gamma_j, \chi_k; \rho_\xi)
\end{aligned} \tag{95}$$

It should be noted that the last term in the bracket in Eq. (93) is only nonzero when $\Lambda = 0$ or 1 and also that because the ρ dependence of the operator factors out, the matrix elements over the $\Phi_{\tau\Lambda}^p(\gamma, \chi; \rho_\xi)$ only need to be evaluated once on each sector.

They are readily evaluated using the PDAF $\Phi_{\tau\Lambda}^p(\gamma, \chi; \rho_\xi)$ and their quadrature points since the PDAF code generates the derivatives of $\Phi_{\tau\Lambda}^p(\gamma, \chi; \rho_\xi)$ directly.

The asymmetric top terms of Eq. (86) can be explicitly written as

$$\begin{aligned}
\langle \tau\Lambda | \frac{1}{2}(A - B)(J_x^2 - J_y^2) | \tau'\Lambda' \rangle &= \frac{1}{4} \hbar^2 \langle \Phi_{\tau\Lambda}^p | A - B | \Phi_{\tau'\Lambda'}^p \rangle [(1 + \delta_{\Lambda 0})(1 + \delta_{\Lambda' 0})]^{-1/2} \\
&\times [\lambda_+(J, \Lambda)\lambda_+(J, \Lambda + 1)\delta_{\Lambda', \Lambda+2} \\
&+ \lambda_-(J, \Lambda)\lambda_-(J, \Lambda - 1)\delta_{\Lambda', \Lambda-2} \\
&+ (-1)^{J+\Lambda+p}\lambda_-(J, \Lambda)\lambda_-(J, \Lambda - 1)\delta_{\Lambda', 2-\Lambda}]
\end{aligned} \tag{96}$$

where

$$A = \frac{1}{\mu\rho_\xi^2(1 + \sin^2\theta)} \tag{97}$$

$$B = \frac{1}{2\mu\rho_\xi^2 \sin^2\theta} \tag{98}$$

$$\begin{aligned}
\langle \Phi_{\tau\Lambda}^p | A - B | \Phi_{\tau'\Lambda'}^p \rangle &= \frac{1}{4} h\pi \Delta\chi \Delta\gamma \sum_{i=1}^{N_x} \sum_{j=1}^{N_\gamma} \sin \gamma_j \sin 2\theta(\gamma_j) \times \\
&\Phi_{\tau\Lambda}^p(\gamma_j, \chi_i; \rho_\xi) (A - B) \Phi_{\tau'\Lambda'}^p(\gamma_j, \chi_i; \rho_\xi)
\end{aligned} \tag{99}$$

The third term in the bracket in Eq. (96) is always zero if $|\Lambda - \Lambda'| > 2$, and the ρ dependence of $A - B$ again factors out, giving the same simplifications and allowing the evaluation of the integrals by the same methods as for the Coriolis terms.

At the boundaries between sectors, the R matrix is transformed by an orthogonal transformation, which requires calculation of the overlap matrix elements. The formula for the overlap matrix elements is given by

$$\begin{aligned}
&\langle \Phi_{\tau\Lambda}^{Jp}(\rho_\xi) | \Phi_{\tau'\Lambda'}^{Jp}(\rho_{\xi'}) \rangle \\
&= \frac{1}{4} h\pi \Delta\chi \Delta\gamma^u \sum_{i=1}^{N_x} \sum_{j=1}^{N_\gamma} \frac{\pi}{4} \sin \gamma_j \sin 2\theta(\gamma_j) \times \\
&\Phi_{\tau\Lambda}^{Jp}(\gamma_j, \chi_i; \rho_\xi) \Phi_{\tau'\Lambda'}^{Jp}(\gamma_j, \chi_i; \rho_{\xi'})
\end{aligned} \tag{100}$$

We compare the computational efficiency of the PDAF, DVR, ABM, and FEM methods on the same computer (PIII 866MHz), by computing eigenvalues, potential matrix elements, and overlap matrices at 100 ρ_ξ 's. ρ_ξ starts from 2.0 a_0 and ends at 9.0 a_0 and is evenly spaced in between. The computation times (CPU time) are shown in Fig. 5.

The FEM method takes much more time than the others, thus we do not include it in Fig. 5. We see that the PDAF method is much faster than the DVR over most of the range of ρ_ξ . If ρ_ξ is very small (less than 2.2 a_0), the DVR is the most efficient method. Although the ABM works slightly faster than the PDAF method, it turns out that the ABM diverges when ρ_ξ is small.

We compare only the potential matrix elements and the overlap matrix elements here, computed using the ABM, DVR and PDAF. The comparison of the potential matrix elements is shown in Fig. 6 and one can see that all the three methods agree with each other very well when $\rho > 3.3a_0$. However, when $\rho < 3.3$, the ABM result diverges from the PDAF and DVR significantly. The comparison of the overlap matrix elements is shown in Fig. 7. One can see clearly from the figure that the PDAF gives results very close to the DVR at small ρ ($\rho < 3.4a_0$), and it also agrees with the ABM very well at large ρ ($\rho > 4.4a_0$). The ABM gives very different results from the PDAF and DVR at small ρ , and DVR gives very different results from

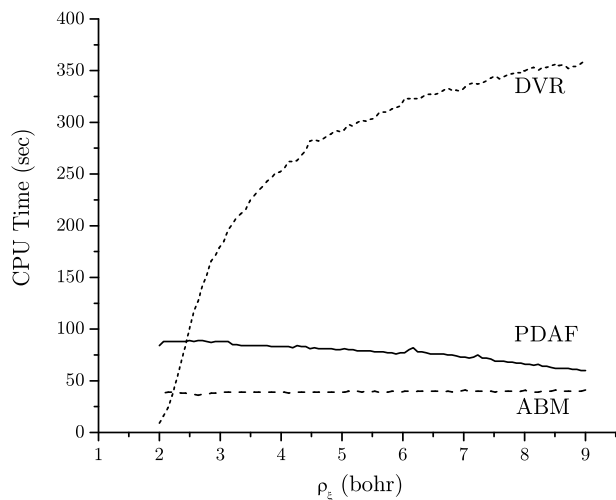


Figure 5: CPU Time of PDAF, DVR and ABM

PDAF and ABM at large ρ . We know that the ABM is very accurate at large ρ and the DVR at small ρ , and thus the comparisons show that the PDAF is accurate both for small and large ρ .

6 Conclusion

In this paper we have presented a periodic distributed approximating functional (PDAF) method for calculating the surface function basis needed in hyperspherical formulations of reactive scattering theory. PDAF functions are introduced and shown to be capable of providing an accurate, efficient representation of the derivative operators.

Test calculations on the $F + H_2$ system with the T5A PES, comparing the PDAF, ABM, DVR and FEM methods showed that the FEM is always the least efficient of the four, and the ABM is the most efficient method for large ρ but is not accurate at small ρ . On the other hand, the DVR is the most efficient method for small ρ but is not accurate for large ρ .

The PDAF is efficient at both large ρ like the ABM and small ρ like the DVR and it is accurate for all ρ . As a result, we find that PDAF is the best method for surface function calculations in hyperspherical reactive scattering calculations.

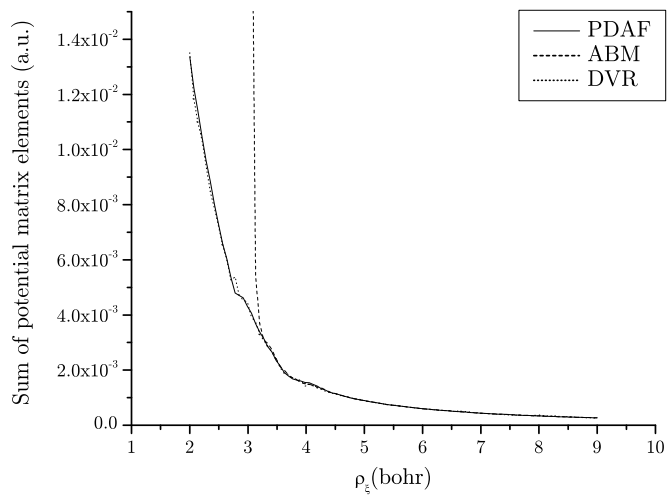


Figure 6: Comparison of the Sum of potential matrix elements using PDAF, ABM and DVR

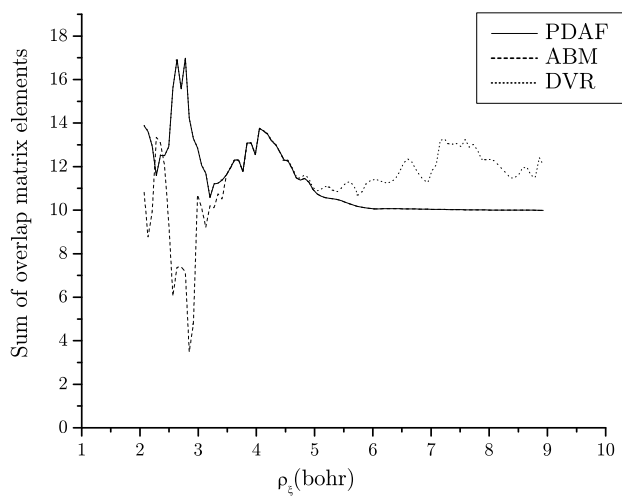


Figure 7: Comparison of the Sum of the overlap matrix elements using PDAF, ABM and DVR.

A H_χ^r is symmetric

$$H_\chi^r(\chi_i, \chi_j) = \sum_R H_\chi(\chi_i, R\chi_j) \Gamma^{[\tau]*}(R) \quad (101)$$

To prove that H_χ^r is symmetric, it is sufficient to show

$$H_{\chi_{\kappa, \kappa'}}^r(\chi_i, \chi_j) = H_{\chi_{\kappa', \kappa}}^r(\chi_j, \chi_i) \quad (102)$$

where

$$H_{\chi_{\kappa, \kappa'}}^r(\chi_i, \chi_j) = \sum_R H_\chi(\chi_i, R\chi_j) \Gamma_{\kappa, \kappa'}^{[z]*}(R) \quad (103)$$

We know that H_χ is symmetric, so

$$\begin{aligned} H_{\chi_{\kappa', \kappa}}^r(\chi_j, \chi_i) &= \sum_R H_\chi(\chi_j, R\chi_i) \Gamma_{\kappa', \kappa}^{[z]*}(R) \\ &= \sum_R H_\chi(R\chi_i, \chi_j) \Gamma_{\kappa', \kappa}^{[z]*}(R) \\ &= \sum_R H_\chi(R^{-1}\chi_i, \chi_j) \Gamma_{\kappa', \kappa}^{[z]*}(R^{-1}) \\ &= \sum_R H_\chi(R^{-1}\chi_i, \chi_j) \Gamma_{\kappa', \kappa}^{[z]*-1}(R) \\ &= \sum_R H_\chi(R^{-1}\chi_i, \chi_j) \Gamma_{\kappa', \kappa}^{[z]*\dagger}(R) \\ &= \sum_R H_\chi(R^{-1}\chi_i, \chi_j) \Gamma_{\kappa, \kappa'}^{[z]}(R) \end{aligned} \quad (104)$$

Because $H_\chi(\chi_i, \chi_j)$ ($DAF^{(2)}(\chi_i - \chi_j)$) depends on $|\chi_i - \chi_j|$, and R is a length-preserving operation, we have

$$\begin{aligned} H_\chi(R^{-1}\chi_j, \chi_i) &= H_\chi(R^{-1}\chi_j, \chi_i) \\ &= H_\chi(RR^{-1}\chi_j, R\chi_i) \\ &= H_\chi(\chi_j, R\chi_i) \end{aligned} \quad (105)$$

Combining (Eq. (104)) and (Eq. (105)) gives

$$H_{\chi_{\kappa, \kappa'}}^r(\chi_i, \chi_j) = \sum_R H_\chi(\chi_i, R\chi_j) \Gamma_{\kappa, \kappa'}^{[z]}(R) \quad (106)$$

Therefore, if $\Gamma^{[z]}$ is real, (Eq. (102)) is true, and H_χ^r is symmetric.

B Irreducible representations of group C_2 , C_{2v} and C_{6v}

The irreducible representation matrices for some point groups frequently used in APH surface function computations are given in Tables Tbl. 7, Tbl. 8 and Tbl. 9. The first column in each table gives the names of the irreducible representations. The second row gives the transformation when a symmetry operation R acts on χ . The parity p is also given in each table.

C_2	E	C_2	p
$R\chi$	χ	$\pi + \chi$	
A	1	1	0
B	1	-1	1

Table 7: Irreducible representations of group C_2

C_{2v}	E	C_2	σ_v	σ'_v	p
$R\chi$	χ	$\pi + \chi$	$2\pi - \chi$	$\pi - \chi$	
A_1	1	1	1	1	0
A_2	1	1	-1	1	0
B_1	1	-1	1	-1	1
B_2	1	-1	-1	1	1

Table 8: Irreducible representations of group C_{2v}

C_{6v}	E	C_6	C_6^5	C_3	C_3^2	C_2	p
$R\chi$	χ	$\frac{\pi}{3} + \chi$	$\frac{5\pi}{3} + \chi$	$\frac{2\pi}{3} + \chi$	$\frac{4\pi}{3} + \chi$	$\pi + \chi$	
A_1	1	1	1	1	1	1	0
A_2	1	1	1	1	1	1	0
B_1	1	-1	-1	1	1	-1	1
B_2	1	-1	-1	1	1	-1	1
E_1	$\begin{pmatrix} 1 & 0 \\ 0 & 1 \end{pmatrix}$	$\begin{pmatrix} \frac{1}{2} & -\frac{\sqrt{3}}{2} \\ \frac{\sqrt{3}}{2} & \frac{1}{2} \end{pmatrix}$	$\begin{pmatrix} \frac{1}{2} & \frac{\sqrt{3}}{2} \\ -\frac{\sqrt{3}}{2} & \frac{1}{2} \end{pmatrix}$	$\begin{pmatrix} -\frac{1}{2} & -\frac{\sqrt{3}}{2} \\ \frac{\sqrt{3}}{2} & -\frac{1}{2} \end{pmatrix}$	$\begin{pmatrix} -\frac{1}{2} & \frac{\sqrt{3}}{2} \\ -\frac{\sqrt{3}}{2} & -\frac{1}{2} \end{pmatrix}$	$\begin{pmatrix} -1 & 0 \\ 0 & -1 \end{pmatrix}$	1
E_2	$\begin{pmatrix} 1 & 0 \\ 0 & 1 \end{pmatrix}$	$\begin{pmatrix} -\frac{1}{2} & -\frac{\sqrt{3}}{2} \\ \frac{\sqrt{3}}{2} & -\frac{1}{2} \end{pmatrix}$	$\begin{pmatrix} -\frac{1}{2} & \frac{\sqrt{3}}{2} \\ -\frac{\sqrt{3}}{2} & -\frac{1}{2} \end{pmatrix}$	$\begin{pmatrix} -\frac{1}{2} & \frac{\sqrt{3}}{2} \\ -\frac{\sqrt{3}}{2} & -\frac{1}{2} \end{pmatrix}$	$\begin{pmatrix} -\frac{1}{2} & -\frac{\sqrt{3}}{2} \\ \frac{\sqrt{3}}{2} & -\frac{1}{2} \end{pmatrix}$	$\begin{pmatrix} 1 & 0 \\ 0 & 1 \end{pmatrix}$	0
R	σ_v	σ'_v	σ''_v	σ_d	σ'_d	σ''_d	p
$R\chi$	$2\pi - \chi$	$\frac{2\pi}{3} - \chi$	$\frac{4\pi}{3} - \chi$	$\frac{\pi}{3} - \chi$	$\pi - \chi$	$\frac{5\pi}{3} - \chi$	
A_1	1	1	1	1	1	1	0
A_2	-1	-1	-1	-1	-1	-1	0
B_1	1	1	1	-1	-1	-1	1
B_2	-1	-1	-1	1	1	1	1
E_1	$\begin{pmatrix} 1 & 0 \\ 0 & -1 \end{pmatrix}$	$\begin{pmatrix} -\frac{1}{2} & \frac{\sqrt{3}}{2} \\ \frac{\sqrt{3}}{2} & \frac{1}{2} \end{pmatrix}$	$\begin{pmatrix} -\frac{1}{2} & -\frac{\sqrt{3}}{2} \\ -\frac{\sqrt{3}}{2} & \frac{1}{2} \end{pmatrix}$	$\begin{pmatrix} \frac{1}{2} & \frac{\sqrt{3}}{2} \\ \frac{\sqrt{3}}{2} & -\frac{1}{2} \end{pmatrix}$	$\begin{pmatrix} -1 & 0 \\ 0 & 1 \end{pmatrix}$	$\begin{pmatrix} \frac{1}{2} & -\frac{\sqrt{3}}{2} \\ -\frac{\sqrt{3}}{2} & -\frac{1}{2} \end{pmatrix}$	1
E_2	$\begin{pmatrix} 1 & 0 \\ 0 & -1 \end{pmatrix}$	$\begin{pmatrix} -\frac{1}{2} & -\frac{\sqrt{3}}{2} \\ -\frac{\sqrt{3}}{2} & \frac{1}{2} \end{pmatrix}$	$\begin{pmatrix} -\frac{1}{2} & \frac{\sqrt{3}}{2} \\ \frac{\sqrt{3}}{2} & \frac{1}{2} \end{pmatrix}$	$\begin{pmatrix} -\frac{1}{2} & \frac{\sqrt{3}}{2} \\ \frac{\sqrt{3}}{2} & \frac{1}{2} \end{pmatrix}$	$\begin{pmatrix} 1 & 0 \\ 0 & -1 \end{pmatrix}$	$\begin{pmatrix} -\frac{1}{2} & -\frac{\sqrt{3}}{2} \\ -\frac{\sqrt{3}}{2} & \frac{1}{2} \end{pmatrix}$	0

Table 9: Irreducible representations of group C_{6v}

References

- [1] See J. M. Bowman, ed., *Advances in Molecular Vibrations and Collision Dynamics*, (JAI, Greenwich, CT, 1994), Volumes 2A and 2B.
- [2] R. E. Wyatt and J. Z. H. Zhang, eds., *Dynamics of Molecules and Chemical Reactions*, (Dekker, New York, 1996).
- [3] H. Nakamura, *Ann. Rev. Phys. Chem.* **48**, 299 (1997).
- [4] G. Nyman and H. G. Wu, *Repts. Progress Physics* **63**, 1 (2000).
- [5] L. D. Faddeev, *Mathematical Aspects of the Three-Body Problem in Quantum Scattering Theory* (Israel Program for Scientific Translation, Jerusalem. Published in the USA by D. Davey & Co., New York, 1965). For a review, see J. C. Y. Chen, *Case Stud. At. Phys.* **3** (5), 305-417 (1973).
- [6] L. M. Delves, *Nucl. Phys.* **9**, 391 (1959); **20**, 275 (1960).
- [7] B. D. Esry, C. H. Greene and J. P. Burke, Jr., *Phys. Rev. Lett.* **83**, 1751 (1999).
- [8] J. M. Launay and M. LeDourneuf, *Chem. Phys. Lett.* **169**, 473 (1990); J. M. Launay, *Theor. Chim. Acta* **79**, 183 (1991).
- [9] R. T Pack, G. A. Parker, *J. Chem. Phys.* **87**, 3888 (1987).
- [10] R. T Pack, G. A. Parker, *J. Chem. Phys.* **90**, 3551 (1989).
- [11] A. Kuppermann and P. G. Hipes, *J. Chem. Phys.* **84**, 5962 (1986); S. A. Cucaro, P. G. Hipes, and A. Kuppermann, *Chem. Phys. Lett.* **154**, 155(1989), **157**, 440 (1989).
- [12] Cf. U. Manthe, T. Seideman, and W. H. Miller, *J. Chem. Phys.* **99**, 10078 (1993); D. Neuhauser, *ibid.* **100**, 92 (1994); D. H. Zhang, and J. Z. H. Zhang, *ibid.* **101**, 1146 (1994); D. H. Zhang and J. C. Light, *ibid.* **105**, 1291 (1996); and W. Zhu, J. Dai, J. Z. H. Zhang, and D. H. Zhang, *ibid.* **105**, 4881 (1996).
- [13] B. Lepetit and J. M. Launay, *J. Chem. Phys.* **95**, 5159 (1991).
- [14] Z. Bačić, J. D. Kress, G. A. Parker, and R. T Pack, *J. Chem. Phys.* **92**, 2344 (1990).
- [15] J. D. Kress, Z. Bačić, G. A. Parker, and R. T Pack, *J. Chem. Phys.* **94**, 8055 (1990).
- [16] J. M. Launay and M. LeDourneuf, *Chem. Phys. Lett.* **163**, 178 (1989).

- [17] J. Linderberg, S. B. Padkjaer, Y. Ohrn, and B. Vessal, *J. Chem. Phys.* **90**, 6254 (1989).
- [18] (a) A. Laganà, R. T Pack, and G. A. Parker, *Faraday Discuss. Chem. Soc.* **84**, 409 (1987); (b) **91**, 386 (1991).
- [19] G. A. Parker, R. T Pack, A. Laganà, B. J. Archer, J. D. Kress,^a and Z. Bačić, in *Super Computer Algorithms for Reactivity, Dynamics and Kinetics of Small Molecules*, edited by A. Laganà (Kluwer, Holland, 1989), p. 105.
- [20] J. D. Kress, Z. Bačić, G. A. Parker, and R. T Pack, *Chem. Phys. Lett.* **157**, 484 (1989).
- [21] J. D. Kress, R. T Pack, G. A. Parker, *Chem. Phys. Lett.* **170**, 306 (1990).
- [22] J. D. Kress, *Chem. Phys. Lett.* **179**, 510 (1991).
- [23] L. Wolniewicz, *J. Chem. Phys.* **90**, 371 (1989);
- [24] G. A. Parker and R. T Pack *J. Chem. Phys.* **98**, 6883 (1993).
- [25] S. S. Iyengar, G. A. Parker, D. J. Kouri, D. K. Hoffman, *J. Chem. Phys.* **110**, 10283 (1999).
- [26] D.K. Hoffman, T.L. Marchioro II, M. Arnold, Y. Huang, W. Zhu and D.J. Kouri, *J. Math. Chem.* **20** (1996) 117-140.
- [27] See Ref. [14] and references therein.
- [28] J. Z. H. Zhang, *Chem. Phys. Lett.* **181**, 63 (1991).
- [29] F. B. Brown, R. Steckler, D. W. Schwenke, D. G. Truhlar, and B. C. Garrett, *J. Chem. Phys.* **82**, 188 (1985); R. Steckler, D. G. Truhlar, and B. C. Garrett, *ibid.* **82**, 5499 (1985).
- [30] M. Weissbluth, *Atoms and Molecules*, Academic Press, INC. (London) Ltd, 1978.
- [31] C. H. Yu, D. J. Kouri, M. Zhao, D. G. Truhlar, and D. W. Schwenke, *Chem. Phys. Lett.* **157**, 491 (1989); *Int. J. Quantum Chem. Symp.* **23**, 45 (1989).
- [32] D. E. Manolopoulos, M. D'Mello, and R. E. Wyatt, *J. Chem. Phys.* **93**, 403 (1990).
- [33] D. Neuhauser, M. Baer, R. S. Judson, and D. J. Kouri, *Chem. Phys. Lett.* **169**, 372 (1990); D. Neuhauser, R. S. Judson, R. L. Jaffe, M. Baer, and D. J. Kouri, *ibid.* **176**, 546 (1991).